JOURNAL OF MATERIALS SCIENCE 33 (1998) 91–97

Formabilities of steel/aluminium alloy laminated composite sheets

H. TAKUDA, H. FUJIMOTO, N. HATTA
Department of Energy Science and Technology, Kyoto University, 606-01 Kyoto, Japan

The tensile properties and press formabilities of laminates experimentally produced from mild steel and various aluminium alloy sheets are examined. The tensile properties of the laminates are approximately predictable by the mixture rule of the properties of the individual sheets. The forming limits in deep drawing, as well as stretch forming due to various types of fractures of the laminated composite sheets, cannot be predicted without considering the stress and strain histories of the individual sheets during forming. Furthermore, it is found that the drawability, as well as the stretch formability, is improved by setting the mild steel sheet on the punch side for the case of aluminium alloy sheet with comparatively high ductility, and by sandwiching the aluminium alloy sheet with the mild steel sheets for the case of low ductility.

1. Introduction

Aluminium alloys are increasingly used in car components to reduce the car weight. Although cast aluminium alloys are used in a considerable number of components, the use of products formed from aluminium alloy sheets is still limited. Aluminium alloy sheets are, normally, inferior to steel sheets in their formability. Therefore, investigations on alloy design are being carried out to obtain aluminium alloy sheets with a high formability as well as high strength [1–3].

On the other hand, laminated composite sheets have been developed and increasingly used in various industries [4]. The desired weight reduction can also be attained by the use of laminates produced from steel and aluminium alloy sheets, and at the same time the formability as well as the strength of aluminium alloy sheets may be compensated for. The mechanical properties of some laminated composite sheets, mainly of stainless steel/aluminium sandwich sheets, have been the subject of examination for many years [5–8]. However, only a few studies have discussed the combination of steel and aluminium alloy sheets from the viewpoint of sheet formability.

In the present study, laminates composed of mild steel and various aluminium alloy sheets are fabricated, and their tensile properties and sheet formabilities are examined. The optimal combination to produce the highest formability and also a predictive method for the formability of the laminated composite sheets are discussed.

2. Materials and laminated composite sheets

The materials used in the present study are three aluminium alloy sheets, AA1100-O, AA2024-T4 and AA5052-O, with a thickness of 1.0 mm, and a mild steel (SPCC) sheet with a thickness of 0.3 mm. Table I lists the chemical compositions of the materials obtained from a chemical analysis.

The laminated composite sheets were fabricated from these materials in the following manner. The aluminium alloy sheets were clad on either one or both sides by the mild steel sheet (Fig. 1). The cladding was performed by adhesive-bonding through a rolling mill using a polyurethane resin. It was observed by microscopic sectional observation of the laminates that there was no thickness change, i.e., no plastic deformation in the aluminium alloy and the steel layers caused by the bonding, and that the thickness of the resin layer ranged between 10–30 μm.

3. Experimental procedures

For the individual mild steel and aluminium alloy sheets and also the laminated composite sheets, the tensile properties and the sheet formabilities in deep drawing and stretch forming were examined by the following tests.

The uniaxial tension tests were performed at 0, 45 and 90° to the rolling direction of the sheet. The width and gauge length of the tensile specimens were set to be 12.5 and 50 mm, respectively.

The cylindrical deep drawing tests were performed using a flat bottomed punch with a diameter of 40 mm and a profile radius of 4 mm. Circular blanks with various diameters with an interval of 1 mm were prepared, and both faces of the blanks were lubricated with sprayed wax. The diameters of the dies were 42.5, 43 and 44 mm for the single layer sheet, the 2-ply and the 3-ply laminates, respectively. The profile radius of each die was 8 mm. The blank holder force for each blank was given according to Siebel's equation [9]. The limiting drawing ratio, (*LDR*), of the laminates

0022–2461

TABLE I Chemical compositions of materials (wt %)

	Si	Fe	Cu	Mn	Mg	Cr	Zn	Ti	Al
AA1100	0.10	0.59	0.14	0.01	0.01	tr.	0.01	0.02	bal.
AA2024	0.07	0.20	4.70	0.58	1.40	0.02	0.04	0.03	bal.
AA5052	0.10	0.26	0.02	0.08	2.45	0.20	0.01	0.01	bal.
	C	Si	Mn	P	S	Al	N	Fe	
SPCC	0.051	0.016	0.220	0.016	0.015	0.025	0.002	bal.	

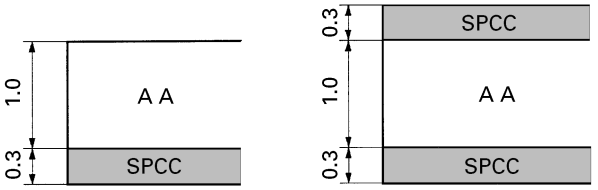

Figure 1 Laminates composed of the mild steel (SPCC) and the aluminium alloy (AA) sheets.

was defined as the ratio of the maximum blank diameter which was drawable without fracture in any layer to the punch diameter.

The Erichsen test used a hemispherical punch with a diameter of 20 mm. Square specimens with a side length of 90 mm were prepared and lubricated with vaseline. The Erichsen value is usually defined as the punch stroke at the fracture observed from the side opposite to the punch. However, all the layers of the laminates do not break at the same time. Due to this the Erichsen value for the laminates is defined in this work as the punch stroke at the fracture of the core layer, i.e. the aluminium alloy layer in principle. In the case where the mild steel layer was set on the die side, the fracture of the aluminium alloy layer could not be observed without fracture of the steel layer. The Erichsen value in this case was exceptionally determined by the fracture of the steel layer on the die side in addition to the fracture of the aluminium alloy layer.

We note that there are two types of deep drawing and Erichsen tests for the 2-ply laminates depending on the setting side. One is the case where the steel and the aluminium alloy layers are set on the punch and the die sides, respectively, and the other is the reverse case.

All the tests were carried out at room temperature for three samples.

4. Results and discussion

4.1. Tensile properties

Table II lists the tensile properties obtained by uniaxial tension tests of the individual sheets. The properties are given with the averages of the data determined at 0, 45 and 90° to the rolling direction, since there was no significant planar anisotropy. The F- and n-values are the parameters in the stress–strain relations that are approximated as:

$$\bar{\sigma} = F\bar{\varepsilon}^n \tag{1}$$

where $\bar{\sigma}$ and $\bar{\varepsilon}$ are the equivalent true stress and strain, respectively.

The three kinds of aluminium alloy sheets have different ductility and strength properties. The proof stress and tensile strength of the AA2024 are larger than those of the mild steel, SPCC. It is characteristic of AA2024 that the fracture occurs without any obvious necking phenomenon and the elongation is small, although the work-hardening exponent, n, is non-negligible. The normal anisotropy parameters, r, of the aluminium alloy sheets are equally small in comparison with that of the steel sheet. The normal anisotropy parameter, r, is defined as:

$$r = \varepsilon_w/\varepsilon_t \tag{2}$$

where ε_w and ε_t are the width and thickness strains of the sheet, respectively.

Figs. 2 and 3 show the proof stresses and the tensile strengths of the laminated composite sheets. The horizontal axis of the figures indicates the ratio of the thickness of the aluminium layer to the total thickness of the laminate. The ratios 1 and 0 mean the individual aluminium alloy and steel sheets, respectively. The proof stresses and the tensile strengths of the laminates closely agree with the values indicated by the dotted lines, namely they obey the following rule of mixtures:

$$Q_L = (Q_A t_A + Q_S t_S)/(t_A + t_S) \tag{3}$$

where Q_A, Q_S and Q_L are the properties of the aluminium alloy, steel and laminated composite sheets, respectively, and t_A and t_S are the thickness values of the aluminium alloy and steel sheets, respectively.

TABLE II Tensile properties.

	AA1100	AA2024	AA5052	SPCC
Proof stress, (MPa)	29	334	97	226
Tensile strength, (MPa)	96	479	202	355
Elongation, (%)	34	17	23	39
Normal anisotropy parameter, r	0.80	0.78	0.72	1.41
F-value ($\bar{\sigma} = F\bar{\varepsilon}^n$), (MPa)	179	749	401	615
Work-hardening exponent, n	0.26	0.19	0.30	0.20

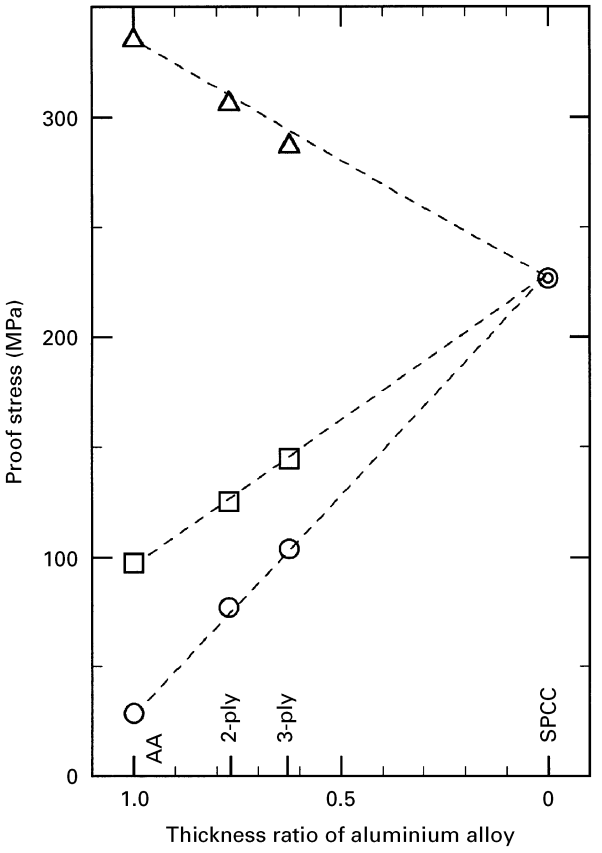

Figure 2 Proof stresses of the individual sheets of mild steel and aluminium alloy and their laminated composite sheets. Key: (○) AA1100, (△) AA2024 and (□) AA5052.

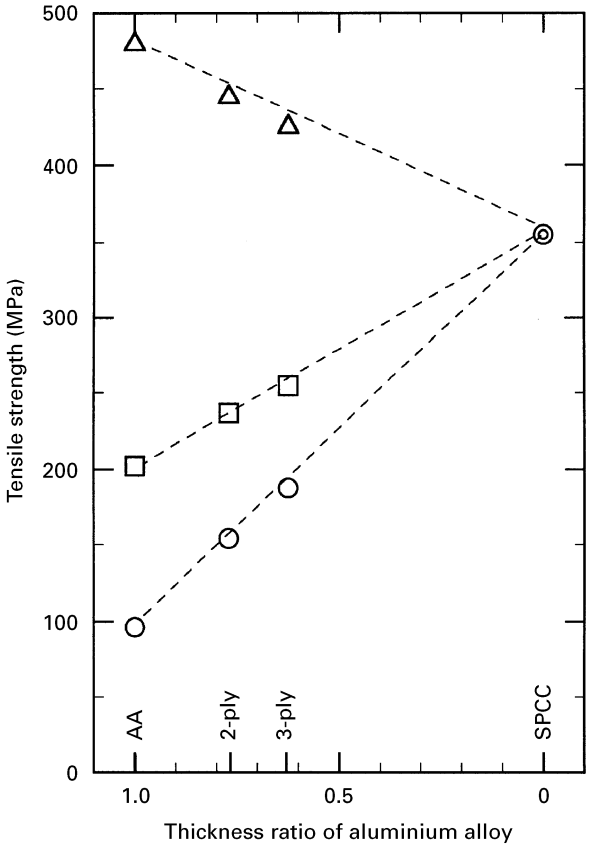

Figure 3 Tensile strengths of the sheets. Key: (○) AA1100, (△) AA2024 and (□) AA5052.

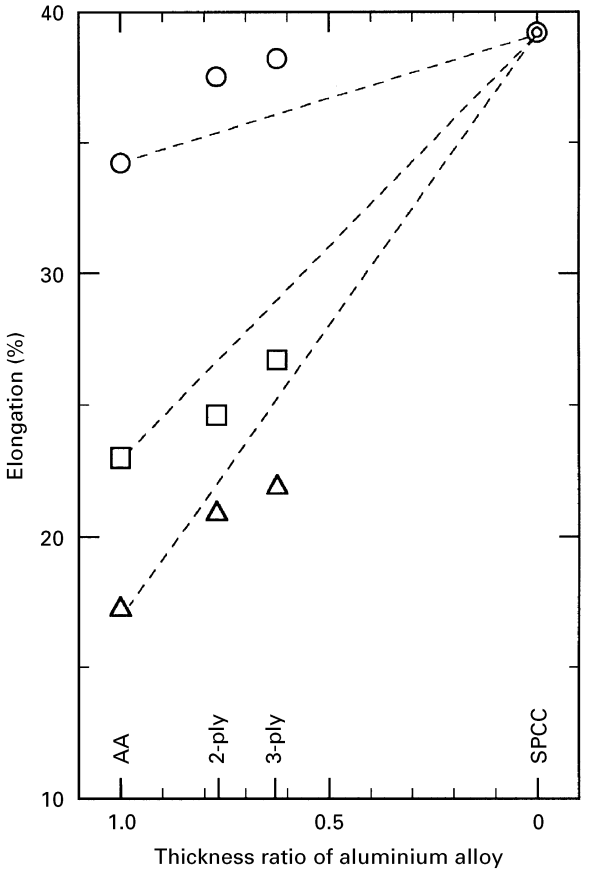

Figure 4 Elongations of the sheets. Key: (○) AA1100, (△) AA2024 and (□) AA5052.

Fig. 4 shows the elongations obtained in the uniaxial tension tests. It is found that the elongation of the aluminium alloy sheet is improved by laminating it with the steel sheet, and that the elongations of the laminates are roughly predictable by the mixture rule.

The normal anisotropy of the laminates could not be accurately measured due to curling phenomenon in the case of 2-ply laminate and the existence of the resin layer between the composing sheets. Therefore, the discussion on the r-value of the laminates is abandoned in the present study. The curling phenomenon is caused by the difference in the r values of the sheets producing the 2-ply laminate [10].

The stress–strain relations of the laminates are approximated by Equation 1, and the F- and n-values are shown in Figs. 5 and 6, respectively. Fig. 5 shows that the mixture rule holds for the F-value. Theoretically, the mixture rule holds for $F\bar{\varepsilon}^n$, not for the individual F- and n-values. Because a great difference in F-values exists between the aluminium alloy and the steel sheets, the n-value does not obey the mixture rule. Fig. 6 shows, however, that it can at least be predicted for the n-value that the tensile properties of the laminated composite sheets exist at a level between the individual properties of the individual aluminium alloy and steel sheets.

4.2. Formabilities in deep drawing and stretch forming

In comparison with the tensile properties in uniaxial deformation, the formabilities in deep drawing and stretch forming are complicated.

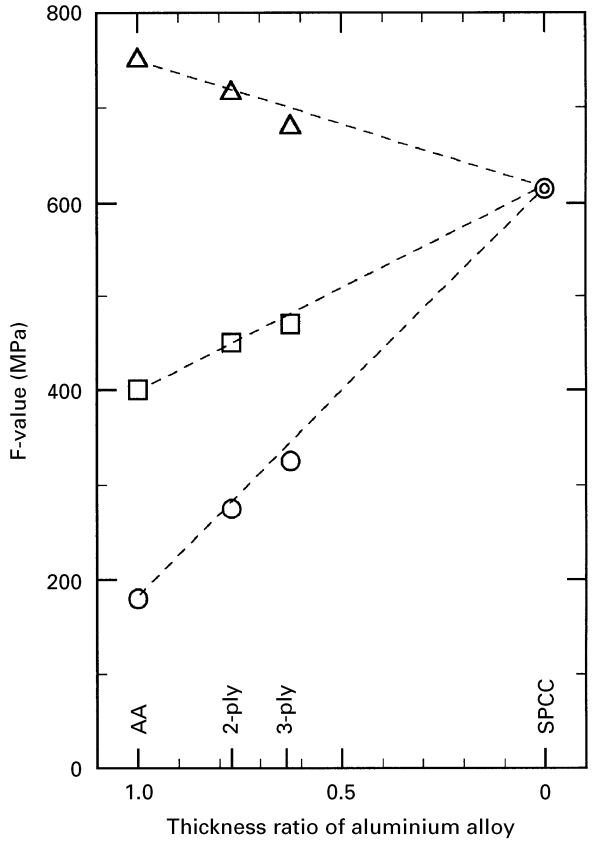

Figure 5 *F*-values of the sheets. Key: (○) AA1100, (△) AA2024 and (□) AA5052.

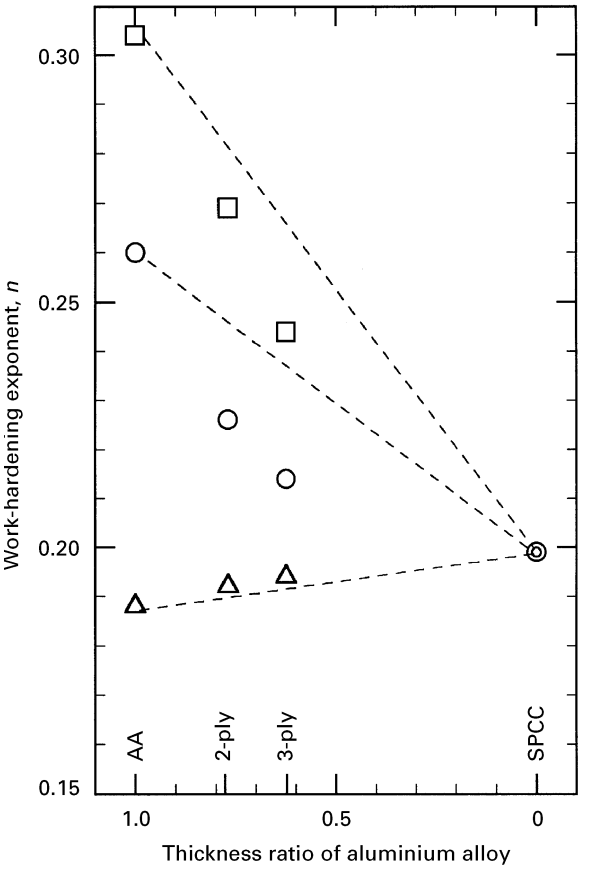

Figure 6 Work-hardening exponents, *n*, of the sheets. Key: (○) AA1100, (△) AA2024 and (□) AA5052.

For example, the limiting drawing ratio, (*LDR*), of the AA1100 sheet with a thickness of 1.0 mm is 2.05, whilst that of the SPCC sheet with a thickness of 0.3 mm is 2.00. The *LDR*s of the laminates produced from the AA1100 and SPCC sheets do not always lie between the values of the individual sheets. Of course there is an influence of the sheet thickness on the LDR in addition to the Erichsen value. However, an important point is that the LDR as well as the Erichsen value of the 2-ply laminate greatly depends upon the setting side, as will be discussed later. For example, the LDR of the laminate produced from the AA1100 and SPCC sheets is 2.18 in the case where the SPCC layer is set on the punch side, while it is 2.00 in the case where the SPCC layer is set on the die side. This shows that the sheet formabilities cannot be simply predicted by the rule of mixtures. Also, there is no simple relation between the sheet formabilities and the tensile properties.

Furthermore, the forming limits in deep drawing and stretch forming depend upon various types of fractures. Fig. 7 (a–c) shows examples of the experimentally observed fractures in deep drawing of the laminated composite sheets. In many cases the fracture in deep drawing occurs at the punch corner, and all the layers of the laminate fracture of this point. However, there are some exceptional cases as is shown in Fig. 7 (a–c).

Fig. 7a shows the outside of the 3-ply laminate SPCC/AA5052/SPCC (initial blank diameter, *d*, = 83 mm) after deep drawing and fracture initiation at the punch corner only in the SPCC layer set on the die side. Fig. 7b shows the fracture at the sidewall in the AA2024 layer on the die side. The limiting drawable diameter of the laminates composed of the AA2024 and SPCC sheets depends on the fracture at the sidewall in the AA2024 layer. There is also the

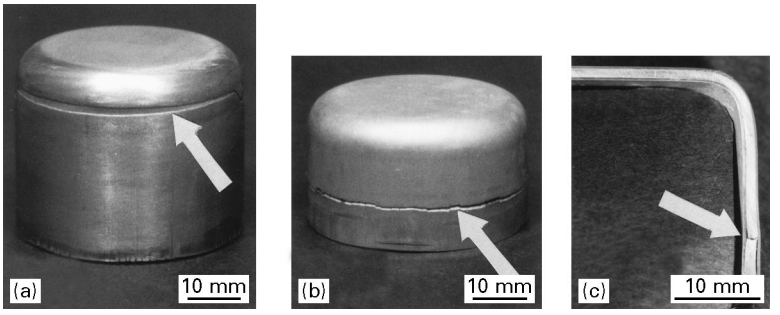

Figure 7 Experimentally observed fractures in deep drawing. (a) SPCC/AA5052/SPCC $d = 83$ mm, (b) SPCC (P)/AA2024 (D) $d = 70$ mm and (c) SPCC/AA2024/SPCC $d = 74$ mm.

TABLE III Fracture strains in tensile direction, ε_{1f}, of materials in uniaxial and plane-strain tension tests

	AA1100	AA2024	AA5052	SPCC
ε_{1f} (uniaxial)	0.62	0.19	0.42	0.77
ε_{1f} (plane-strain)	0.42	0.14	0.29	0.35

TABLE IV The material specific constants a and b in Equation 4

	AA1100	AA2024	AA5052	SPCC
a	0.33	0.61	0.30	0.057
b	0.42	0.18	0.28	0.29

case where the fracture cannot be observed without sectioning of the sample. Fig. 7c shows the section of the laminate SPCC/AA2024/SPCC ($d = 74$ mm) after deep drawing. It is observed that the fracture occurs only in the centre layer, i.e. the AA2024 layer at the sidewall.

In order to predict the forming limits due to such various types of fractures, it may be important to analyse the deformation history of each sheet.

At this point, we would like to apply a criterion for ductile fracture to predict the formabilities in deep drawing and stretch forming of the laminated composite sheets. Based on various hypotheses, several criteria for ductile fracture have been proposed [11]. The occurrence of ductile fracture in these criteria is estimated by the macroscopic stress and strain during forming. Since the distributions of stress and strain are calculated in a finite element simulation, the fracture initiation can be predicted by means of a combination of the finite element simulation and the criteria for ductile fracture.

In the present study, we employ the following criterion proposed by Oyane *et al.* [12]:

$$\int_0^{\bar{\varepsilon}_f} \left(\frac{\sigma_m}{\bar{\sigma}} + a \right) d\bar{\varepsilon} = b \tag{4}$$

where $\bar{\varepsilon}_f$ is the equivalent strain at which the fracture occurs, σ_m is the hydrostatic stress, and a and b are material specific constants.

To determine these material specific constants plane-strain tension tests were performed in addition to the uniaxial tension tests. Table III lists the fracture strains in the tensile direction, ε_{1f}, derived from the measured reductions of area in uniaxial and plane-strain tension tests.

When the normal sheet anisotropy is considered in accordance with Hill's yield criterion [13], the ratios of the hydrostatic stress to the equivalent stress, $\sigma_m/\bar{\sigma}$, and of the equivalent strain to the strain in tensile direction, $\bar{\varepsilon}/\varepsilon_1$, during uniform deformation at the uniaxial and plane-strain tension tests are given as:

$$\frac{\sigma_m}{\bar{\sigma}} = \frac{1}{3}\left(\frac{2(2+r)}{3(1+r)} \right)^{1/2}, \quad \frac{\bar{\varepsilon}}{\varepsilon_1} = \left(\frac{2(2+r)}{3(1+r)} \right)^{1/2} \quad \text{(uniaxial)} \tag{5}$$

and

$$\frac{\sigma_m}{\bar{\sigma}} = \frac{1}{3}\left(\frac{2(2+r)(1+2r)}{3(1+r)} \right)^{1/2}, \quad \frac{\bar{\varepsilon}}{\varepsilon_1} = \left(\frac{2(2+r)(1+r)}{3(1+2r)} \right)^{1/2} \quad \text{(plane-strain)} \tag{6}$$

Provided that the relations in Equations 5 and 6 are maintained until the fracture that is initiated though the necking influences the stress and strain after uniform deformation, the material constants a and b can be approximately obtained by use of Equations 4–6 and ε_{1f} in Table III, as is indicated in Table IV.

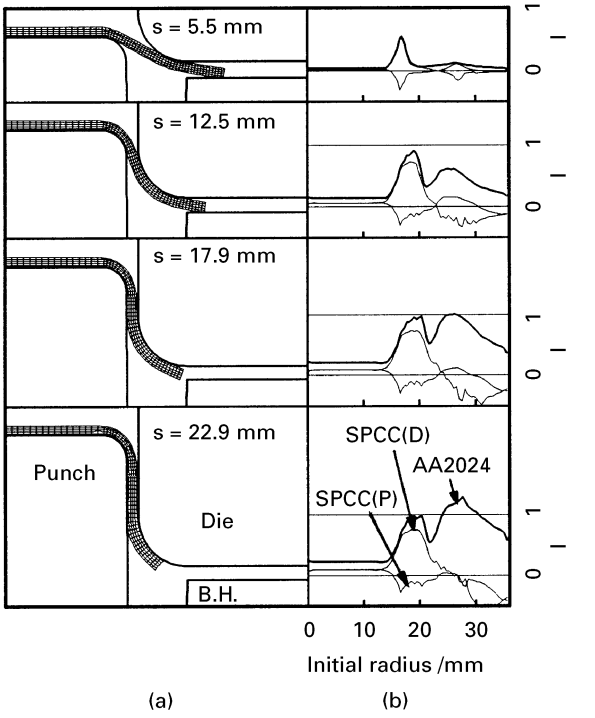

Figure 8 (a) Deformed meshes and (b) distributions of the integral I in deep drawing calculated for the SPCC/AA2024/SPCC laminate ($d = 74$ mm).

Using the values of the a and b constants listed in Table IV and the stress and strain histories calculated by finite element simulation, the forming limit in sheet forming can be predicted by Equation 4. The literature [14, 15] should be referred to for the simulation method. In addition to the a and b material specific constants the tensile properties of the individual sheets, such as F-, n- and r-values in Table II, are used in the finite element simulation.

Fig. 8 (a and b) illustrates, as an example, the calculated result of deep drawing for the case of the 3-ply laminate SPCC/AA2024/SPCC shown in Fig. 7c. Fig. 8a shows the transition of the sectional blank profile with an increase in the punch stroke, s. The calculated result of the ductile fracture criterion is shown in Fig. 8b, using the integral I modified from Equation 4,

$$I = \frac{1}{b}\int_0^{\bar{\varepsilon}} \left(\frac{\sigma_m}{\bar{\sigma}} + a \right) d\bar{\varepsilon} \tag{7}$$

The condition of fracture is satisfied when and where the integral I is equal to 1.

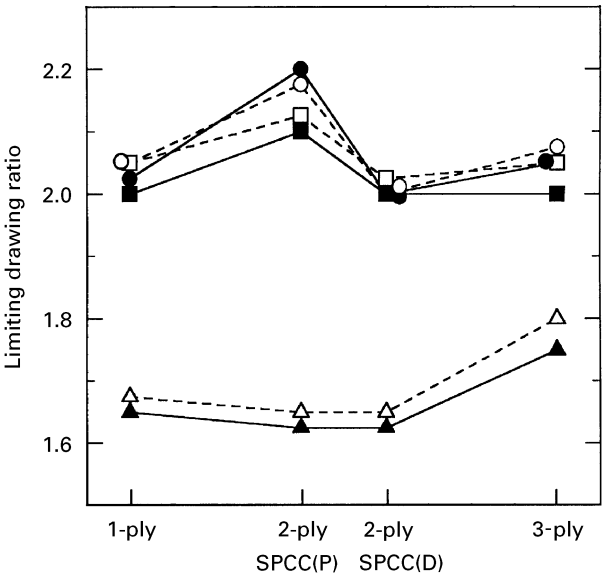

Figure 9 Limiting drawing ratios of the aluminium alloy and the laminated sheets. Key: AA1100: (○) experimental, (●) calculated, AA5052: (□) experimental, (■) calculated, AA2024: (△) experimental, (▲) calculated.

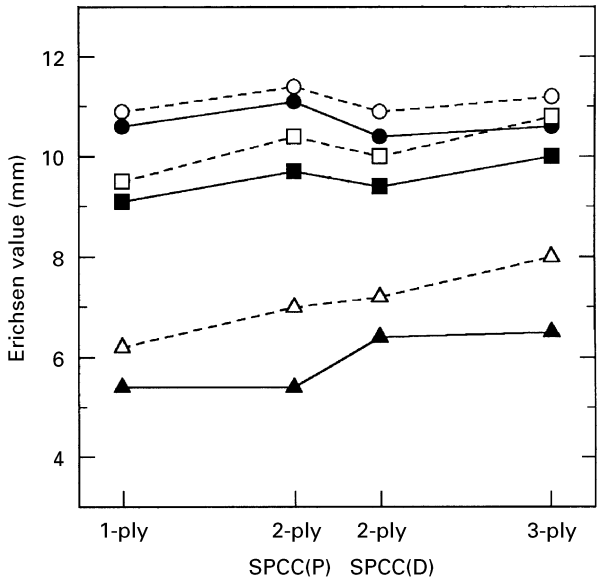

Figure 10 Erichsen values of the aluminium alloy and the laminated sheets. Key: AA1100: (○) experimental, (●) calculated, AA5052: (□) experimental, (■) calculated, AA2024: (△) experimental, (▲) calculated.

The horizontal and vertical axes of Fig. 8(b) indicate the initial radial position from the blank centre and the value of I at the corresponding radial position of each layer of the laminate, respectively. In the AA2024 layer as well as the SPCC layer on the die side, the integral I at the punch corner increases during the early stage of deep drawing, but it does not reach 1. On the other hand, the integral I at the sidewall of the AA2024 layer increases mainly during the later stage, until fracture occurs there. The calculated result closely corresponds to the experimentally observed fracture of Fig. 7c.

Figs. 9 and 10 show the limiting drawing ratios and the Erichsen values of the three aluminium alloy sheets and their laminates with the mild steel sheets. The forming limits predicted by means of the ductile fracture criterion are indicated by the solid marks. Good agreements are obtained between the calculated and experimental results. It is found from both the experimental and calculated results that for the aluminium alloy sheets with comparatively high ductility, AA1100 and AA5052, the LDR and the Erichsen value are improved for the case of 2-ply laminate where the SPCC layer is set on the punch side. For the aluminium alloy sheet with low ductility, AA2024, an improvement in formability is observed for the 3-ply laminate.

5. Conclusions

In the present study, the tensile properties and sheet formabilities of various aluminium alloy sheets clad by mild steel sheets were examined. The results are summarized as follows:

(1) The tensile properties of the laminated composite sheets can be approximately given by the rule of mixtures, i.e. the average of the component properties weighted by volume fractions.

(2) There is no simple relation between the tensile properties and the sheet formabilities in deep drawing and stretch forming. The forming limits due to various types of fractures of the laminated composite sheets cannot be predicted by the mixture rule.

(3) The forming limits are predictable from the tensile properties of the individual sheets on condition that the histories of stress and strain during forming are considered, e.g., by the combination of a finite element simulation and the ductile fracture criterion.

(4) For the aluminium alloy sheets with comparatively high ductility, AA1100 and AA5052, the drawability as well as the stretch formability is improved for the case of a 2-ply laminate where the mild steel layer is set on the punch side.

(5) For the aluminium alloy sheet with low ductility, AA2024, the formability is improved by sandwiching the AA2024 sheet between the mild steel sheets.

Acknowledgements

The authors would like to thank SKY Aluminium Co. Ltd and Nippon Steel Corporation for supplying the test materials. The authors are grateful also to Mr. M. Tanaka in the Graduate School of Kyoto University for his assistance with the laboratory work.

References

1. T. KOMATSUBARA and M. MATSUO, *SAE Tech. Paper No. 890712* (1989).
2. H. HOSOMI, *Sumitomo Light Metal Technical Reports* **32** (1991) 1.
3. M. YANAGAWA and S. OIE, *J. Jpn. Inst. Light Metals* **41** (1991) 119.
4. A. YAHIRO, T. MASUI, T. YOSHIDA and D. DOI, *ISIJ Int.* **31** (1991) 647.
5. R. HAWKINS and J. C. WRIGHT, *J. Inst. Metals* **99** (1971) 357.

6. M. HIRAIWA and K. KONDO, *Bull. JSME* **20** (1977) 483.
7. S. L. SEMIATIN and H. R. PIEHLER, *Metall. Trans. A* **10A** (1979) 85.
8. D. N. LEE and Y. K. KIM, *J. Mater. Sci.* **23** (1988) 558.
9. E. SIEBEL, *Stahl Eisen* **74** (1954) 155.
10. F. YOSHIDA and Y. OHSAWA, *J. JSTP* **32** (1990) 94.
11. S. E. CLIFT, P. HARTLEY, C. E.N. STURGESS and G. W. ROWE, *Int. J. Mech. Sci.* **32** (1990) 1.
12. M. OYANE, T. SATO, K. OKIMOTO and S. SHIMA, *J. Mech. Work Technol.* **4** (1980) 65.
13. R. HILL, in "Mathematical theory of plasticity", (Oxford University Press, 1950) p. 318.
14. K. MORI and H. TAKUDA, *Trans. NAMRI/SME* **24** (1996) 143.
15. H. TAKUDA, K. MORI, H. FUJIMOTO and N. HATTA, *J. Mater. Process. Technol.* **60** (1996) 291.

Received 9 September 1996
and accepted 4 August 1997